ACS OMEGA

Open Access

http://pubs.acs.org/journal/acsodf

Article

Fullerene-Based Heterojunctions for Non-Selective Absorption Transparent Solar Cells

Ruiqian Meng, Qianqing Jiang, and Dianyi Liu*

Cite This: *ACS Omega* 2024, 9, 25960−25967

Read Online

ACCESS | Metrics & More | Article Recommendations | Supporting Information

ABSTRACT: Transparent photovoltaic (TPV) devices have great potential to be applied as smart windows in construction and agriculture fields. TPVs with an average visible transmission (AVT) exceeding 50% are among the strong candidates to build lighting windows since the champion efficiency has already exceeded 10%. However, it is still a challenge in TPVs that semiconductors are generally expensive and transparency is difficult to further enhance, particularly for device AVT exceeding 70%. In this work, we develop a set of fullerene-based heterojunctions to harvest the light. By utilizing the low-cost fullerene as the light-absorbing material and combining it with the transparent electrode, the fabricated TPV device can achieve an AVT of 72.1% with a PCE exceeding 1%. Notably, the device with an AVT of 82% is also successfully demonstrated. This study provides an effective approach for building low-cost and efficient TPV devices.

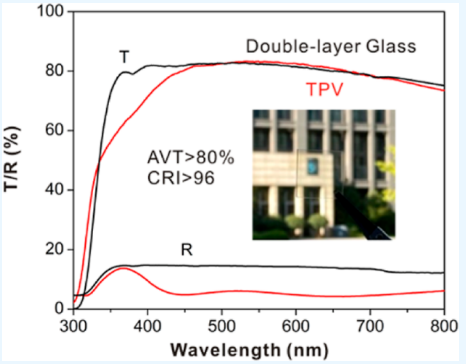

INTRODUCTION

Transparent photovoltaic (TPV) is a promising technique for building-integrated photovoltaic (BIPV) fields. It is envisaged to replace traditional building materials such as glass curtain walls, exterior wall decorative stones, and roof tiles.[1−3] TPV devices with the average visible transmission (AVT) of over 50% can supply electricity with little impact on human vision.[4−7] Especially, devices with AVT exceeding 70% can approach the transparency level of double-layer architectural glass, further expanding their practical applications. However, achieving a device AVT over 70% is highly challenging due to the main hurdle in the design of light-absorption materials.

The development of TPV devices encompasses various fields including organic solar cells, dye-sensitized solar cells,[8] perovskite solar cells,[9,10] and luminescent solar concentrators.[11] Among these, the rapid development of light-absorption materials in organic solar cells has led to significant improvement in device photovoltaic performance. Combined with the lightweight and flexible advantages of organic photovoltaics, transparent organic devices demonstrate strong potential for various applications.[12−14] One of the effective strategies for constructing highly transparent organic TPVs is to utilize wavelength-selective absorption semiconductors as light-harvesting materials, including ultraviolet (UV)- and near-infrared (NIR)-selective semiconductors.[2,15−17] For example, the TPV based on PDTP-DFBT:FOIC as NIR-absorption materials is reported to achieve a device PCE of 3.5% and an AVT of 61.5%.[18] The NIR-selective-absorption PTB7-Th:6TIC-4F and UV-selective-absorption perovskite are combined to fabricate tandem TPV devices, exhibiting an efficiency of over 10% with an AVT of 52.9%.[19] An NIR/UV-absorption ClAlPc/C_{60} heterojunction is introduced to fabricate TPV and the device achieves a PCE of 1.34% and an AVT of 77.45%.[20] The UV-absorption organic molecular donors are synthesized to act as light-harvesting semiconductors in TPVs, and the device achieves an AVT of up to 80.3% and a PCE of 0.61%.[21] These progresses greatly encourage research in the TPV field. However, the molecular structures and synthesis processes of wavelength-selective semiconductors are generally complex, which indicates that the manufacturing costs of TPVs will be significantly raised. Therefore, developing low-cost semiconductors and constructing efficient heterojunctions is an inevitable way to apply the TPVs in the commercial field.

Fullerene compounds, a category of carbon-based semiconductors, possess both excellent photovoltaic capabilities and are cost-effective. Previous research studies have reported that fullerene and its derivatives can not only serve as critical components for electron acceptors and electron transport layers but also significantly impact photon absorption and photocurrent generation in solar cells.[22,23] Herein, we adopted fullerene molecules as the primary light-harvesting materials and developed a set of efficient heterojunctions to apply in TPV devices. By investigating the various fullerene-based heterojunctions and finely optimizing the fullerene film

Received: January 24, 2024
Revised: April 3, 2024
Accepted: May 23, 2024
Published: June 5, 2024

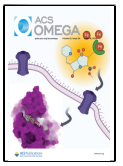

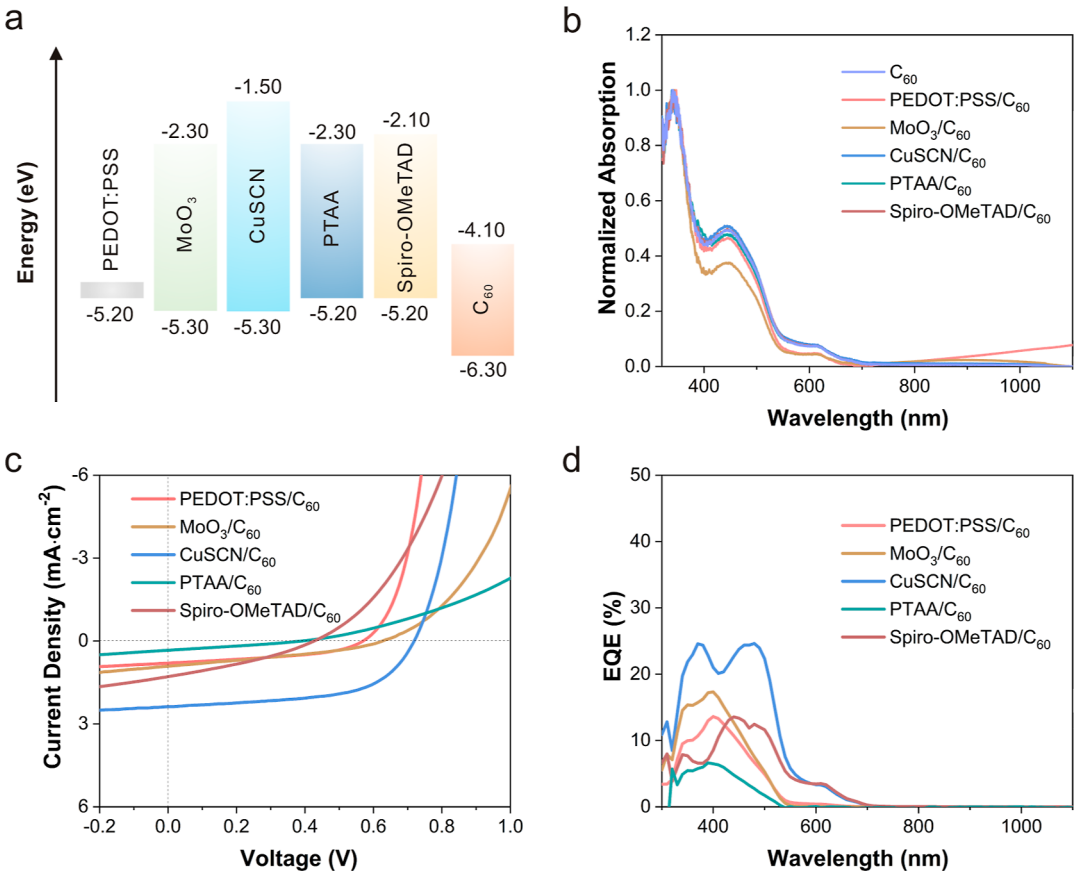

Figure 1. (a) Energy levels of the materials applied in the various heterojunctions. (b) Absorption spectra of various heterojunction films on quartz glasses. (c) *J*–*V* and (d) EQE curves of opaque devices based on various heterojunctions.

thickness, TPVs can achieve the AVT (spectral range from 430 to 670 nm) of up to 82%. The superior transparency of TPV devices rivals that of window glass, positioning them as among the most transparent photovoltaic devices. Notably, despite the limited absorption of fullerene in the visible-light range, the outstanding copper thiocyanate (CuSCN)/fullerene heterojunction enables TPV devices to maintain a PCE of over 1%, even with an AVT exceeding 70%. This work may promote the development of low-cost, non-selective semiconductor materials in TPV.

RESULTS AND DISCUSSION

Due to the excellent electron-extraction capability, fullerene compounds are well known in the organic photovoltaic field. Firdaus and his colleagues found that fullerene works very well as a light-absorption semiconductor and the device shows an efficiency of over 6%.[24] By reducing the thickness of the fullerene layer, the fullerene film is expected to be used in a transparent device. The creative work opens the door to developing efficient fullerene-based TPV devices. However, since fullerene molecules usually act as n-type semiconductors, a suitable p-type semiconductor is needed to form an efficient heterojunction. The fullerene-based heterojunctions have not been well developed.

Here, we use fullerene C_{60} as a reference fullerene molecule to carry out the research of fullerene-based heterojunctions because the thickness of the C_{60} film can be easily controlled by the thermal evaporation method. Five commonly used hole transfer materials (HTMs) in organic photovoltaics are employed as p-type semiconductors to form C_{60}-based heterojunctions (Figure 1a,b). All energy level values are sourced from the literature.[24−27] In addition to PEDOT:PSS, four other materials can form type-II heterojunctions with C_{60} to promote the effective separation of electrons and holes in space. The absorption peaks of these heterojunction films are comparable to those of the corresponding C_{60} films, indicating that C_{60} plays the primary role in light absorption. To investigate the role of various heterojunctions in solar cells, opaque devices are constructed with the structure of ITO/PEDOT:PSS/HTM/C_{60}/BCP/Ag. Figure 1c and Table S1 illustrate the device performance with various HTMs/C_{60} heterojunctions. CuSCN/C_{60}-based devices show a maximum PCE of 0.981% and a J_{SC} of 2.38 mA cm^{-2}. The exceptional device performance based on CuSCN/C_{60} primarily arises from the charge generation process analogous to the observed emissive charge transfer state in the organic−inorganic heterojunctions, promoting efficient charge separation.[28] The external quantum efficiency (EQE) characterization reveals that the CuSCN/C_{60}-based device has relatively strong absorption, suggesting higher charge generation and separation efficiency at the CuSCN/C_{60} interface (Figure 1d).[29] In contrast, the EQE curves of other devices suggest a lack of appropriate charge separation interfaces. Additionally, EQE spectra of all devices show that charge generation occurs mainly focused on the spectral range of less than 550 nm. This also indirectly reflects that C_{60} might be a suitable semiconductor for fabricating highly transparent devices. Thus, we subsequently attempted to construct TPVs using the efficient CuSCN/C_{60} heterojunction.

https://doi.org/10.1021/acsomega.4c00823
ACS Omega 2024, 9, 25960−25967

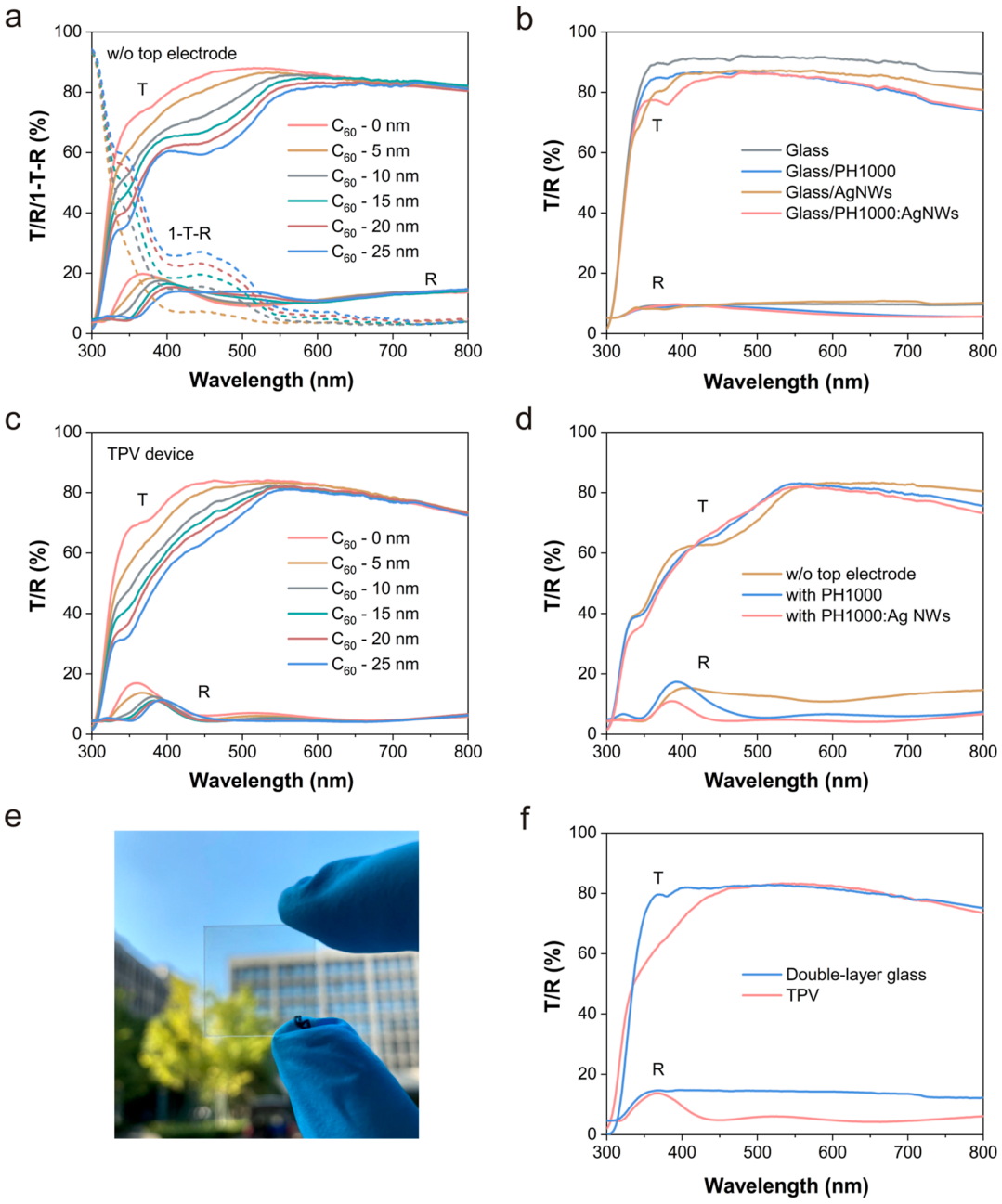

Figure 2. Optical properties of related samples. (a) Transmission (T)/reflection (R)/1−T−R spectra of the ITO/PEDOT:PSS/CuSCN/C_{60}/BCP sample with various thicknesses of C_{60} films (0−25 nm). (b) T/R spectra of the different electrode materials on glass substrates. (c) T/R spectra of TPV devices with the C_{60} film thicknesses from 0 to 25 nm. (d) T/R spectra for the C_{60}−20 nm TPV devices with different top electrodes. (e) Photograph of the C_{60}−20 nm TPV device with the top electrode. (f) T/R spectra of double-layer glass and the C_{60}−5 nm TPV device.

Table 1. Optical Parameters of ITO/PEDOT:PSS/CuSCN/C_{60}/BCP Samples and TPV Devices with Various Thicknesses of C_{60} Films

samples	parameters	0 nm	5 nm	10 nm	15 nm	20 nm	25 nm
without top electrode	AVT (%)	86.9	85.6	84.0	82.1	79.9	77.6
	CRI	98.7	96.9	96.8	94.9	94.0	86.2
	CIE (a*, b*)	−1.75, 0.18	−1.88, 2.64	−1.20, 8.31	−0.04, 11.88	0.38, 13.73	1.52, 16.01
TPV device	AVT (%)	83.2	82.6	81.2	80.4	80.2	78.9
	CRI	98.8	98.2	95.4	93.6	96.8	95.7
	CIE (a*, b*)	−1.32, 0.47	−1.35, 1.27	−2.03, 4.33	−2.02, 6.48	−2.00, 8.68	−2.10, 11.49

The structure of ITO/PEDOT:PSS/CuSCN/C_{60}/BCP is employed to investigate the sample transparency without depositing the top electrode. As shown in Figure 2a and Table 1, with the increasing thickness of the C_{60} film (0−25 nm), the absorption of corresponding samples gradually rises. Meanwhile, a slight increase in reflection at the visible-light region

https://doi.org/10.1021/acsomega.4c00823
ACS Omega 2024, 9, 25960−25967

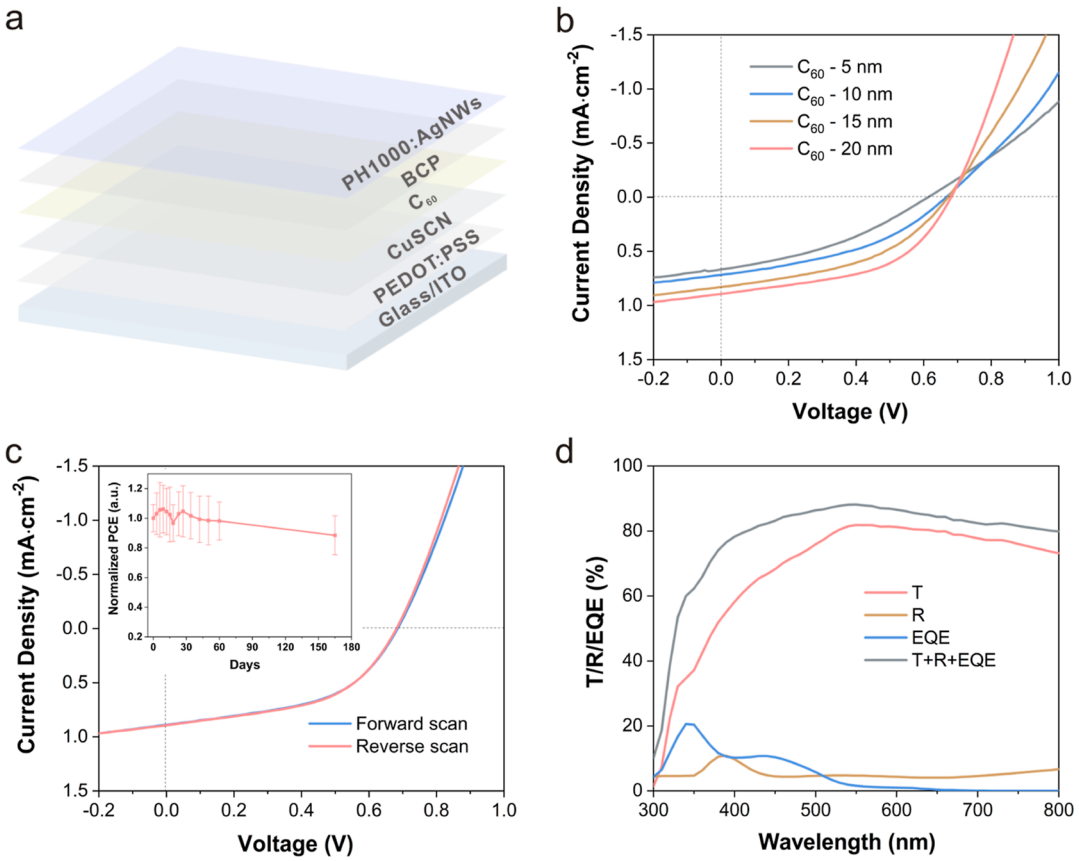

Figure 3. Performance characteristics of TPV devices. (a) Architecture of the TPV device. (b) *J*−*V* characteristics for TPV devices with different thicknesses of C_{60}. (c) *J*−*V* curves from forward scan and reverse scan for the C_{60}−20 nm TPV device. The inset of (c) device stability of C_{60}−20 nm TPV. (d) *T*/*R*/EQE properties for the corresponding C_{60}−20 nm TPV device.

leads to a notable reduction in overall transmission. Most samples exhibit AVT over 80%, and the sample with the C_{60}−5 nm film shows the highest AVT of 85.6%. When the thickness of the C_{60} film reaches 20 nm, the AVT of the sample without the top electrode reaches the critical boundary of 80%. According to the above results, the thicknesses of C_{60} films in TPV devices are limited to lower than 20 nm in the following experiments, which is expected to achieve TPV with AVT over 80%. In addition, the morphology of C_{60} films with different thicknesses is also researched (Figure S1). As confirmed by atomic force microscopy (AFM) characterization, the thickness changes have no evident influence on the final morphology and roughness of the C_{60} film.

The transparent electrode is another crucial factor for TPVs.[30−32] Besides the highly transparent ITO, highly conductive PH1000 can also serve as the transparent electrode with the room-temperature lamination transfer technique.[33−37] This method can protect the underlying layers from fabrication damage.[38,39] Furthermore, the silver nanowires (Ag NWs) solution is added to the PH1000 precursor to reduce the sheet resistance from 141 ± 31 to 84 ± 22 Ω/sq. As shown in Figure 2b and Table S2, the introduction of Ag NWs primarily affects the transmittance within the 340−420 nm range, avoiding the region of human eye visual response. The AVT of the PH1000 and PH1000:Ag NWs hybrid film shows close values of 84.9 and 85.0%, respectively. Therefore, it has a negligible effect on film transparency. The electrode morphology is tested by scanning electron microscopy (SEM) (Figure S2). Randomly cross-linked Ag NWs are built with a low coverage ratio so that it may favor the transmission of incident light.[40] The combination of high conductivity and transparency makes the PH1000:Ag NWs hybrid film a strong contender as a transparent electrode in the TPV field.

By laminating the PH1000:Ag NWs transparent top electrode (Figure S3), the TPV devices with CuSCN/C_{60} heterojunctions are successfully fabricated with the structure of ITO/PEDOT:PSS/CuSCN/C_{60}/BCP/PH1000:Ag NWs. The SEM images of the sample before and after loading the top electrode are shown in Figure S4. A staggered arrangement of Ag NWs on the organic layer is well observable, and the morphology of the PH1000:Ag NWs electrode remains relatively consistent after depositing. Optical properties of TPVs are shown in Figure 2c, Table 1, and Figure S5. When the C_{60} thickness is no more than 20 nm, all TPV devices exhibit the AVT exceeding 80%. In addition, for C_{60}-20 nm and C_{60}-25 nm films, the AVT values of related TPV devices are even higher than the samples without the top electrode. Take the C_{60}−20 nm film as an example, after depositing the PH1000:Ag NWs electrode, the transmission of the TPV device in the range of 420−590 nm is higher than the device without the top electrode, resulting in a noticeable improvement of the AVT (Figure 2d). It can be inferred that the transmission improvement stems from the antireflection effect of the PH1000:Ag NWs electrode. The reflection of the TPV device is significantly lower than the samples without the top electrode, indicating that more photons can go into/through the TPV device. This antireflection effect can offset the photon

https://doi.org/10.1021/acsomega.4c00823
ACS Omega 2024, 9, 25960−25967

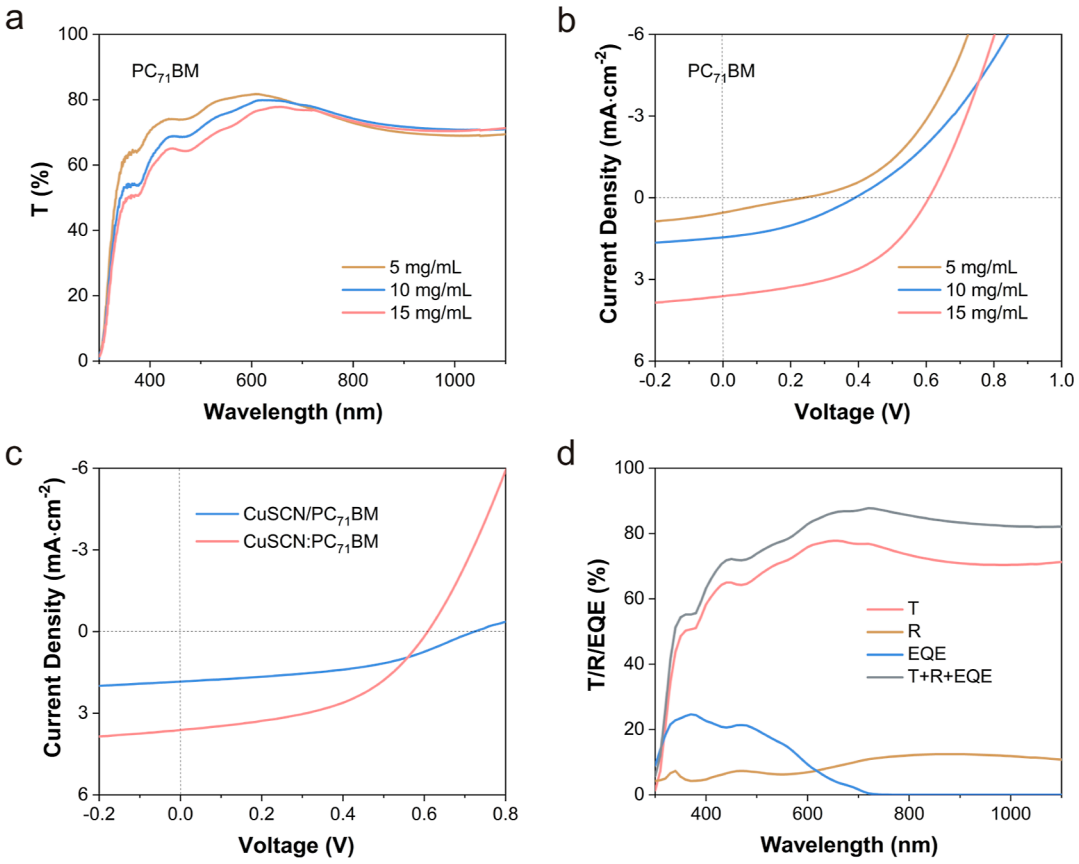

Figure 4. Performance characteristics of $PC_{71}BM$-based TPV devices. (a) *T* and (b) *J*−*V* curves of TPV devices based on a CuSCN:$PC_{71}BM$ blend layer (concentration of $PC_{71}BM$ is 5/10/15 mg/mL). (c) *J*−*V* curves of TPV devices based on the CuSCN/$PC_{71}BM$ bilayer and the CuSCN:$PC_{71}BM$ blend layer (concentration of $PC_{71}BM$ is 15 mg/mL). (d) *T*/*R*/EQE properties for the corresponding CuSCN:$PC_{71}BM$ TPV device (concentration of $PC_{71}BM$ is 15 mg/mL).

loss by electrode absorption and result in higher transmission.[41−43]

Notably, the color rendering index (CRI) of TPV devices is up to 98, which indicates that the devices are almost colorless and show the minimum impact on vision.[9,44] As shown in Figure 2e, the C_{60}−20 nm TPV device looks clear and substantially transparent, and the colors of all objects are well maintained. Double-layer glass (microscope slides used as a reference) is a commonly used material for building windows, so it serves as a reference to describe the transparency of highly transparent TPVs (Figure 2f). CuSCN/C_{60}-based TPV devices present an AVT of 80.2−82.6% and CRI of 93−98, which are comparable with double-layer microscope slides (AVT of 82% and CRI of 99.1). The highly transparent TPVs essentially match the optical requirements for application on window glass in architecture.

After confirming that the TPV device meets transparency requirements, we explored the photovoltaic performance of the devices with the structure shown in Figures 3a and S6. *J*−*V* curves and performance parameters are summarized in Figures 3b, S7, and Table S3. The device PCE exhibits an upward trend with an increased thickness of C_{60}. This result largely depends on the light-absorption capacity of the active layer, which can also be confirmed in the 1-*T*−*R* curves of C_{60} films. The PCE of the champion TPV is up to 0.31%, with an open-circuit voltage (V_{OC}) of 0.680 V, a short-circuit current density (J_{SC}) of 0.893 mA cm^{-2}, and a fill factor of 50.3%. Meanwhile, the forward and reverse scan curves almost coincide, which is serviceable in proving the good fabrication of the TPV device (Figure 3c). In addition, the integrated J_{EQE} is 0.85 mA cm^{-2}, which matches well with the J_{SC} obtained by the *J*−*V* measurement and further verifies the performance of the device. To satisfy the photon balance consistency check,[45] the optical properties of the TPV devices are systematically researched. As shown in Figure 3d, the *T*, *R*, and EQE curves of the complete device are summarized. It can be proved that EQE + *T* + *R* < 100% in all spectral ranges. Thus, so far, we have achieved CuSCN/C_{60}-based TPV devices with AVT exceeding 80% and a PCE of 0.31%.

Device stability is also an important factor in evaluating the device performance and potential application. Therefore, the efficiency stability of unencapsulated TPV devices (stored in the glovebox) is shown in the inset of Figure 3c. The results show that tested devices can maintain a PCE over 80% of the initial efficiency after 60 days. Even after 165 days, the device PCE still achieves more than 75% of the initial PCE. The stability of the device may largely be attributed to the stability of active materials and the stable CuSCN/C_{60} heterojunction. Moreover, the fabrication method of the device structure is simple and can satisfy the requirements for the fabrication of large-area devices. As shown in Figure S8 and Table S4, the efficiency of the corresponding large-area device remains at the same level as the small-area device.

Considering that the transparent electrode can significantly impact device transparency and photovoltaic performance, we tried to introduce the commonly used top electrode to

https://doi.org/10.1021/acsomega.4c00823
ACS Omega 2024, 9, 25960−25967

investigate device photovoltaic performance while maintaining high transparency (Figure S9 and Table S5). The opaque silver electrode is also adopted as the reference for the transparent electrodes. Related device performances are summarized in Figure S10 and Table S6. The opaque device presents the highest efficiency, and the photocurrent is higher than that of the transparent devices. It is easily understood that the active layer reabsorbs the reflective light reflected by the opaque silver electrode and contributes to the high photocurrent. The thin-silver-film transparent electrode device exhibits improved performance (PCE = 0.355%) compared to the PH1000-based TPV devices. Owing to the strong reflection in the range of 530−800 nm, the transparency of the thin-silver-film transparent electrode is significantly decreased, resulting in the AVT of the device of only 69.4%. The device with the PH1000-only transparent electrode shows a comparable AVT to the device with the PH1000:Ag NWs hybrid electrode. However, the PCE is lower than that of the PH1000:Ag NWs-based TPV device due to the higher sheet resistance.

Since fullerene molecules are highly soluble in organic solvents, we can also employ the solution process to prepare the fullerene-based heterojunction, including planar heterojunction structure and bulk-heterojunction structure. Previous study suggests that the bulk-heterojunction structure (CuSCN:PCBM) has improved charge separation performance compared to the planar structured heterojunction (CuSCN/PCBM). Therefore, we fabricated the TPV device with CuSCN and (6,6)-phenyl C71 butyric acid methyl ester ($PC_{71}BM$) bulk heterojunction by the solution process, and the device with the CuSCN/$PC_{71}BM$ planar heterojunction was also prepared for comparison. Photovoltaic and optical performances of the TPV devices are summarized in Figures 4 and S11 and Table S7−S9. Consistent with the opaque device results in the literature, the TPV with the CuSCN:$PC_{71}BM$ blend layer heterojunction shows improved performance than the planar heterojunction device.[23] With $PC_{71}BM$ precursor concentration of 15 mg/mL, TPV with the blend layer heterojunction can achieve the AVT of 72.1% and the PCE of 1.05% (Figure 4d), and the thicknesses of CuSCN:$PC_{71}BM$ bulk heterojunction and $PC_{71}BM$ in the bilayer heterojunction are 66.4 ± 3.3 and 22.7 ± 1.8 nm, respectively. It is worth mentioning that, despite the device performances that are comparable to the TPVs with other light-absorption materials, such as perovskite, metal halide, and synthesized organic small-molecule semiconductors,[9,10,21,44] the low performance is challenging to meet practical application requirements. This is primarily attributed to the inherent contradiction between active-layer light absorption and light transmission as well as the impact of high-transparency electrodes on device optical absorption. Nonetheless, the results indicate again that the fullerenes are promising candidates for the light-harvesting materials of efficient TPVs.

In the devices based on CuSCN/C_{60} and CuSCN:$PC_{71}BM$ heterojunctions, CuSCN:$PC_{71}BM$-based devices demonstrate relatively higher photovoltaic performance. Besides differences in photon absorption capability, heterojunction electron and hole mobilities are also conducted (Figure S12). By space charge-limited current measurements, electron and hole mobilities for CuSCN/C_{60} are determined to be 1.14×10^{-5} and 8.32×10^{-6} cm^2 V^{-1} S^{-1}, respectively, whereas CuSCN:$PC_{71}BM$ exhibits relatively balanced charge carrier mobilities, with electron and hole mobilities calculated as 3.45×10^{-6} and 3.94×10^{-6} cm^2 V^{-1} S^{-1}, respectively. This further indicates reduced charge carrier recombination in CuSCN:$PC_{71}BM$-based devices, thereby enhancing the photovoltaic performance.

As one of the excellent hole transport materials, the hole transport properties of the CuSCN have already been finely studied in previous reports.[23] When the bottom PEDOT:PSS layer is removed, the photovoltaic performance and optical properties of the device are still comparable with those of the fully structured device (Figures S13 and S14 and Table S10, S11). Therefore, CuSCN is used not only to construct the heterojunction with fullerene molecules but also be considered to work as the hole transport layer in this study.

CONCLUSIONS

In summary, we demonstrate a set of fullerene-based heterojunctions to act as light-absorption materials in TPVs. Fullerene derivatives not only promote efficient charge generation and transport but also offer versatile processing methods and demonstrate excellent chemical stability and cost-effectiveness. The non-wavelength-selective fullerene-based heterojunctions can efficiently absorb and convert the light to electricity while exhibiting a high light transmittance. We summarized the parameters of reported TPV cells in recent years with AVT > 50% in Figure S15 and Table S12. The results show that research on highly transparent TPVs is increasing dramatically, and the AVT has rapidly enhanced from ∼ 60% to over 80% in recent years. However, balancing transparency and efficiency is still challenging in the TPV field, especially for highly transparent TPVs. This study indicates that non-wavelength-selective semiconductors can also be employed to fabricate highly transparent TPVs. The fullerene-based heterojunction TPVs exhibit performance comparable to other materials when the AVT exceeds 70%. The high transparency of TPVs is even comparable with the double-layer glass, which is broadly used as the window in the architecture field. While the PCE of highly transparent devices may not be as satisfactory, this work opens the possibility of utilizing non-wavelength-selective semiconductors in high-transparency devices, encouraging powering smart buildings while meeting the high aesthetic requirements of practical applications.

ASSOCIATED CONTENT

Supporting Information

The Supporting Information is available free of charge at https://pubs.acs.org/doi/10.1021/acsomega.4c00823.

Experimental details of device fabrication and characterization. AFM, top-view SEM, schematic diagram, statistical graphs and summary of device parameters, and summary of reported TPV cells with over 50% of AVT (PDF)

AUTHOR INFORMATION

Corresponding Author

Dianyi Liu − *Key Laboratory of 3D Micro/Nano Fabrication and Characterization of Zhejiang Province, Research Center for Industries of the Future and School of Engineering, Westlake University, Hangzhou, Zhejiang 310030, China; Institute of Advanced Technology, Westlake Institute for Advanced Study, Hangzhou, Zhejiang 310024, China;* orcid.org/0000-0001-7288-1108; Email: liudianyi@westlake.edu.cn

https://doi.org/10.1021/acsomega.4c00823
ACS Omega 2024, 9, 25960−25967

Authors

Ruiqian Meng − *Key Laboratory of 3D Micro/Nano Fabrication and Characterization of Zhejiang Province, Research Center for Industries of the Future and School of Engineering, Westlake University, Hangzhou, Zhejiang 310030, China; Institute of Advanced Technology, Westlake Institute for Advanced Study, Hangzhou, Zhejiang 310024, China*

Qianqing Jiang − *Key Laboratory of 3D Micro/Nano Fabrication and Characterization of Zhejiang Province, Research Center for Industries of the Future and School of Engineering, Westlake University, Hangzhou, Zhejiang 310030, China; Institute of Advanced Technology, Westlake Institute for Advanced Study, Hangzhou, Zhejiang 310024, China*

Complete contact information is available at: https://pubs.acs.org/10.1021/acsomega.4c00823

Funding

This work was supported by the Westlake Education Foundation.

Notes

The authors declare the following competing financial interest(s): R. M., Q. J. and D.L. have filed a patent application based on the work in this manuscript.

■ ACKNOWLEDGMENTS

We thank the facility support and technical assistance from the Instrumentation and Service Center for Physical Sciences (ISCPS), as well as from the Center for Micro/Nano Fabrication at Westlake University.

■ REFERENCES

(1) Wang, W.; Yan, C.; Lau, T. K.; Wang, J.; Liu, K.; Fan, Y.; Lu, X.; Zhan, X. Fused hexacyclic nonfullerene acceptor with strong near-infrared absorption for semitransparent organic solar cells with 9.77% efficiency. *Adv. Mater.* **2017**, *29*, 1701308.

(2) Traverse, C. J.; Pandey, R.; Barr, M. C.; Lunt, R. R. Emergence of highly transparent photovoltaics for distributed applications. *Nat. Energy* **2017**, *2*, 849−860.

(3) Chang, S.-Y.; Cheng, P.; Li, G.; Yang, Y. Transparent polymer photovoltaics for solar energy harvesting and beyond. *Joule* **2018**, *2*, 1039−1054.

(4) Davy, N. C.; Sezen-Edmonds, M.; Gao, J.; Lin, X.; Liu, A.; Yao, N.; Kahn, A.; Loo, Y.-L. Pairing of near-ultraviolet solar cells with electrochromic windows for smart management of the solar spectrum. *Nat. Energy* **2017**, *2*, 17104.

(5) Lunt, R. R. Theoretical limits for visibly transparent photovoltaics. *Appl. Phys. Lett.* **2012**, *101*, 043902.

(6) Rahmany, S.; Etgar, L. Semitransparent perovskite solar cells. *ACS Energy Lett.* **2020**, *5*, 1519−1531.

(7) Lunt, R. R.; Bulovic, V. Transparent, near-infrared organic photovoltaic solar cells for window and energy-scavenging applications. *Appl. Phys. Lett.* **2011**, *98*, 113305.

(8) Naim, W.; Novelli, V.; Nikolinakos, I.; Barbero, N.; Dzeba, I.; Grifoni, F.; Ren, Y.; Alnasser, T.; Velardo, A.; Borrelli, R.; Haacke, S.; Zakeeruddin, S. M.; Graetzel, M.; Barolo, C.; Sauvage, F. Transparent and colorless dye-sensitized solar cells exceeding 75% average visible transmittance. *JACS Au* **2021**, *1*, 409−426.

(9) Liu, D.; Yang, C.; Lunt, R. R. Halide perovskites for selective ultraviolet-harvesting transparent photovoltaics. *Joule* **2018**, *2*, 1827−1837.

(10) Liu, T.; Zhao, X.; Wang, P.; Burlingame, Q. C.; Hu, J.; Roh, K.; Xu, Z.; Rand, B. P.; Chen, M.; Loo, Y. L. Highly transparent, scalable, and stable perovskite solar cells with minimal aesthetic compromise. *Adv. Energy Mater.* **2022**, *13*, 2200402.

(11) Yang, C.; Sheng, W.; Moemeni, M.; Bates, M.; Herrera, C. K.; Borhan, B.; Lunt, R. R. Ultraviolet and near-infrared dual-band selective-harvesting transparent luminescent solar concentrators. *Adv. Energy Mater.* **2021**, *11*, 2003581.

(12) Li, X.; Tang, A.; Wang, H.; Wang, Z.; Du, M.; Guo, Q.; Guo, Q.; Zhou, E. Benzotriazole-Based 3D Four-Arm Small Molecules Enable 19.1% Efficiency for PM6: Y6-Based Ternary Organic Solar Cells. *Angew. Chem., Int. Ed.* **2023**, *62*, No. e202306847.

(13) Dai, T.; Tang, A.; He, Z.; Du, M.; Lei, P.; Zeng, Q.; Wang, Z.; Wang, Y.; Lu, S.; Zhong, Y.; Zhou, E. Modulating intermolecular interactions by collaborative material design to realize THF-processed organic photovoltaic with 1.3 V open-circuit voltage. *Energy Environ. Sci.* **2023**, *16*, 2199−2211.

(14) Wang, D.; Liu, H.; Li, Y.; Zhou, G.; Zhan, L.; Zhu, H.; Lu, X.; Chen, H.; Li, C.-Z. High-performance and eco-friendly semi-transparent organic solar cells for greenhouse applications. *Joule* **2021**, *5*, 945−957.

(15) Hu, Z.; Wang, J.; Ma, X.; Gao, J.; Xu, C.; Wang, X.; Zhang, X.; Wang, Z.; Zhang, F. Semitransparent organic solar cells exhibiting 13.02% efficiency and 20.2% average visible transmittance. *J. Mater. Chem. A* **2021**, *9*, 6797−6804.

(16) Lopez-Garcia, A. J.; Bauer, A.; Fonoll Rubio, R.; Payno, D.; Jehl Li-Kao, Z.; Kazim, S.; Hariskos, D.; Izquierdo-Roca, V.; Saucedo, E.; Pérez-Rodríguez, A. Uv-selective optically transparent Zn(O,S)-based solar cells. *Sol. RRL* **2020**, *4*, 2000470.

(17) Meng, R.; Jiang, Q.; Liu, D. Balancing efficiency and transparency in organic transparent photovoltaics. *npj Flexible Electron.* **2022**, *6*, 39.

(18) Xie, Y.; Xia, R.; Li, T.; Ye, L.; Zhan, X.; Yip, H. L.; Sun, Y. Highly transparent organic solar cells with all-near-infrared photoactive materials. *Small Methods* **2019**, *3*, 1900424.

(19) Zuo, L.; Shi, X.; Fu, W.; Jen, A. K. Y. Highly efficient semitransparent solar cells with selective absorption and tandem architecture. *Adv. Mater.* **2019**, *31*, 1901683.

(20) Li, M. Z.; Lee, C. C.; Biring, S.; Hsu, I. S.; Luo, D.; Estrada, R.; Wu, Y. S.; Yang, C. C.; Liu, S. W. Vacuum-deposited transparent organic photovoltaics for efficiently harvesting selective ultraviolet and near-infrared solar energy. *Sol. RRL* **2021**, *5*, 2000564.

(21) Ball, M. L.; Burlingame, Q.; Smith, H. L.; Liu, T.; Parkin, S. R.; Kahn, A.; Loo, Y.-L. Design of UV-absorbing donor molecules for nearly imperceptible organic solar cells. *ACS Energy Lett.* **2022**, *7*, 180−188.

(22) Karuthedath, S.; Gorenflot, J.; Firdaus, Y.; Sit, W.-Y.; Eisner, F.; Seitkhan, A.; Ravva, M. K.; Anthopoulos, T. D.; Laquai, F. Charge and triplet exciton generation in neat $PC_{70}BM$ films and hybrid CuSCN:$PC_{70}BM$ solar cells. *Adv. Energy Mater.* **2019**, *9*, 1802476.

(23) Firdaus, Y.; Seitkhan, A.; Eisner, F.; Sit, W.-Y.; Kan, Z.; Wehbe, N.; Balawi, A. H.; Yengel, E.; Karuthedath, S.; Laquai, F.; Anthopoulos, T. D. Charge photogeneration and recombination in mesostructured CuSCN-nanowire/$PC_{70}BM$ solar cells. *Sol. RRL* **2018**, *2*, 1800095.

(24) Sit, W.-Y.; Eisner, F. D.; Lin, Y.-H.; Firdaus, Y.; Seitkhan, A.; Balawi, A. H.; Laquai, F.; Burgess, C. H.; McLachlan, M. A.; Volonakis, G.; Giustino, F.; Anthopoulos, T. D. High-efficiency fullerene solar cells enabled by a spontaneously formed mesostructured CuSCN-nanowire heterointerface. *Adv. Sci.* **2018**, *5*, 1700980.

(25) Pattanasattayavong, P.; Yaacobi-Gross, N.; Zhao, K.; Ndjawa, G. O. N.; Li, J.; Yan, F.; O'Regan, B. C.; Amassian, A.; Anthopoulos, T. D. Hole-transporting transistors and circuits based on the transparent inorganic semiconductor copper(I) thiocyanate (CuSCN) processed from solution at room temperature. *Adv. Mater.* **2013**, *25*, 1504−1509.

(26) Cokduygulular, E.; Cetinkaya, C.; Emik, S.; Kinaci, B. In-depth analysis on PTB7 based semi-transparent solar cell employing MoO_3/Ag/WO_3 contact for advanced optical performance and light utilization. *Sci. Rep.* **2023**, *13*, 7548.

(27) Zhang, M.; Hu, W.; Shang, Y.; Zhou, W.; Zhang, W.; Yang, S. Surface passivation of perovskite film by sodium toluenesulfonate for highly efficient solar cells. *Sol. RRL* **2020**, *4*, 2000113.
(28) Eisner, F.; Foot, G.; Yan, J.; Azzouzi, M.; Georgiadou, D. G.; Sit, W. Y.; Firdaus, Y.; Zhang, G.; Lin, Y. H.; Yip, H. L.; Anthopoulos, T. D.; Nelson, J. Emissive charge-transfer states at hybrid inorganic/organic heterojunctions enable low non-radiative recombination and high-performance photodetectors. *Adv. Mater.* **2022**, *34*, 2104654.
(29) Wijeyasinghe, N.; Regoutz, A.; Eisner, F.; Du, T.; Tsetseris, L.; Lin, Y.-H.; Faber, H.; Pattanasattayavong, P.; Li, J.; Yan, F.; McLachlan, M. A.; Payne, D. J.; Heeney, M.; Anthopoulos, T. D. Copper(I) thiocyanate (CuSCN) hole-transport layers processed from aqueous precursor solutions and their application in thin-film transistors and highly efficient organic and organometal halide perovskite solar cells. *Adv. Funct. Mater.* **2017**, *27*, 1701818.
(30) Kim, Y.; Ryu, T. I.; Ok, K.-H.; Kwak, M.-G.; Park, S.; Park, N.-G.; Han, C. J.; Kim, B. S.; Ko, M. J.; Son, H. J.; Kim, J.-W. Inverted Layer-By-Layer Fabrication of an Ultraflexible and Transparent Ag Nanowire/Conductive Polymer Composite Electrode for Use in High-Performance Organic Solar Cells. *Adv. Funct. Mater.* **2015**, *25*, 4580−4589.
(31) Fang, Y.; Wu, Z.; Li, J.; Jiang, F.; Zhang, K.; Zhang, Y.; Zhou, Y.; Zhou, J.; Hu, B. High-Performance Hazy Silver Nanowire Transparent Electrodes through Diameter Tailoring for Semi-transparent Photovoltaics. *Adv. Funct. Mater.* **2018**, *28*, 1705409.
(32) Sun, Y.; Chang, M.; Meng, L.; Wan, X.; Gao, H.; Zhang, Y.; Zhao, K.; Sun, Z.; Li, C.; Liu, S.; Wang, H.; Liang, J.; Chen, Y. Flexible organic photovoltaics based on water-processed silver nanowire electrodes. *Nat. Electron.* **2019**, *2*, 513−520.
(33) Wang, X.; Ishwara, T.; Gong, W.; Campoy-Quiles, M.; Nelson, J.; Bradley, D. D. C. High-Performance Metal-Free Solar Cells Using Stamp Transfer Printed Vapor Phase Polymerized Poly(3,4-Ethylenedioxythiophene) Top Anodes. *Adv. Funct. Mater.* **2012**, *22*, 1454−1460.
(34) Qin, F.; Wang, W.; Sun, L.; Jiang, X.; Hu, L.; Xiong, S.; Liu, T.; Dong, X.; Li, J.; Jiang, Y.; Hou, J.; Fukuda, K.; Someya, T.; Zhou, Y. Robust metal ion-chelated polymer interfacial layer for ultraflexible non-fullerene organic solar cells. *Nat. Commun.* **2020**, *11*, 4508.
(35) Gupta, D.; Wienk, M. M.; Janssen, R. A. J. Efficient Polymer Solar Cells on Opaque Substrates with a Laminated PEDOT:PSS Top Electrode. *Adv. Energy Mater.* **2013**, *3*, 782−787.
(36) Sun, L.; Zeng, W.; Xie, C.; Hu, L.; Dong, X.; Qin, F.; Wang, W.; Liu, T.; Jiang, X.; Jiang, Y.; Zhou, Y. Flexible All-Solution-Processed Organic Solar Cells with High-Performance Nonfullerene Active Layers. *Adv. Mater.* **2020**, *32*, 1907840.
(37) Jiang, Y.; Liu, T.; Zhou, Y. Recent Advances of Synthesis, Properties, Film Fabrication Methods, Modifications of Poly(3,4-ethylenedioxythiophene), and Applications in Solution-Processed Photovoltaics. *Adv. Funct. Mater.* **2020**, *30*, 2006213.
(38) Zhao, Z.; Liu, M.; Yang, K.; Xu, C.; Guan, Y.; Ma, X.; Wang, J.; Zhang, F. Highly Sensitive Narrowband Photomultiplication-Type Organic Photodetectors Prepared by Transfer-Printed Technology. *Adv. Funct. Mater.* **2021**, *31*, 2106009.
(39) Zhou, Y.; Khan, T. M.; Shim, J. W.; Dindar, A.; Fuentes-Hernandez, C.; Kippelen, B. All-plastic solar cells with a high photovoltaic dynamic range. *J. Mater. Chem. A* **2014**, *2*, 3492−3497.
(40) Yu, S.; Li, J.; Zhao, L.; Wu, M.; Dong, H.; Li, L. Simultaneously enhanced performances of flexible CuNW networks by covering ATO layer for polymer solar cells. *Sol. Energy Mater. Sol. Cells* **2021**, *221*, 110885.
(41) Sun, Z.; He, Y.; Xiong, B.; Chen, S.; Li, M.; Zhou, Y.; Zheng, Y.; Sun, K.; Yang, C. Performance-enhancing approaches for PEDOT:PSS-Si hybrid solar cells. *Angew. Chem., Int. Ed.* **2021**, *60*, 5036−5055.
(42) Yan, W.; Qu, Y.; Gupta, T. D.; Darga, A.; Nguyên, D. T.; Page, A. G.; Rossi, M.; Ceriotti, M.; Sorin, F. Semiconducting nanowire-based optoelectronic fibers. *Adv. Mater.* **2017**, *29*, 1700681.
(43) Ahn, J.; Hwang, H.; Jeong, S.; Moon, J. Metal-nanowire-electrode-based perovskite solar cells: Challenging issues and new opportunities. *Adv. Energy Mater.* **2017**, *7*, 1602751.
(44) Liu, D.; Yang, C.; Chen, P.; Bates, M.; Han, S.; Askeland, P.; Lunt, R. R. Lead halide ultraviolet-harvesting transparent photovoltaics with an efficiency exceeding 1%. *ACS Appl. Energy Mater.* **2019**, *2*, 3972−3978.
(45) Yang, C.; Liu, D.; Bates, M.; Barr, M. C.; Lunt, R. R. How to accurately report transparent solar cells. *Joule* **2019**, *3*, 1803−1809.

https://doi.org/10.1021/acsomega.4c00823
ACS Omega 2024, 9, 25960−25967